Comparison of force fields for the prediction of thermophysical properties of long linear and branched alkanes

Sebastian Schmitt, Florian Fleckenstein, Hans Hasse, and Simon Stephan*

Laboratory of Engineering Thermodynamics (LTD), RPTU Kaiserslautern, Kaiserslautern 67663, Germany

E-mail: simon.stephan@rptu.de

Abstract

The prediction of thermophysical properties at extreme conditions is an important application of molecular simulations. The quality of these predictions primarily depends on the quality of the employed force field. In this work, a systematic comparison of classical transferable force fields for the prediction of different thermophysical properties of alkanes at extreme conditions, as they are encountered in tribological applications, was carried out using molecular dynamics simulations. Nine transferable force fields from three different classes were considered (all-atom, united-atom, and coarse-grained force fields). Three linear alkanes (n-decane, n-icosane, and n-triacontane) and two branched alkanes (1-decene trimer and squalane) were studied. Simulations were carried out in a pressure range between 0.1 and 400 MPa at 373.15 K. For each state point, density, viscosity, and self-diffusion coefficient were sampled, and the results were compared to experimental data. The Potoff force field yielded the best results.

Introduction

Thermophysical properties of lubricants at extreme pressures are highly important for the design of processes in mechanical engineering.[1] Especially the density and the transport properties determine the performance of the lubricant in the lubrication gap. The pressure in tribological systems with small contact areas are often higher than 1,000 MPa.[2] For such conditions, experimental data are rare due to high costs and complexity of the measurements.[3] Hence, reliable predictive models are needed. Molecular simulation is an attractive method for this.

Molecular dynamics (MD) simulations have been used often for the prediction of thermophysical bulk properties of lubricants,[4–11] wetting, and interfacial properties on solid walls,[12–15] as well as for the simulation of tribological contact processes.[16–23] Simulations of lubricants usually aim at predicting transport properties, in particular the viscosity, using either equilibrium molecular dynamics (EMD)[24–28] or non-equilibrium molecular dynamics (NEMD) simulations.[7,29–32] Both methods are challenging: EMD simulations require a large computational effort to compute the viscosity, especially for higher viscosities due to the slow convergence of the auto correlation function (ACF).[33] In NEMD simulations, the shear rate has to be small enough to reach the Newtonian regime which can require very long simulation times due to the bad signal-to-noise ratio at small shear rates.[34] As the viscosity becomes very large at high pressures,[35] the prediction of transport properties at high pressures is a challenging task with high computational costs. Special methods have been applied for tackling this task, such as the time decomposition method.[33]

MD simulations of lubricants require force fields that model the inter- and intramolecular interactions. Especially for the quantitative prediction of bulk properties, the choice of an adequate force field is crucial. There is a large number of different force fields that can be used for modeling lubricants.[36–38] The choice of the force field is not trivial as different force fields have different strengths and weaknesses, and comparisons on equal terms are usually difficult from the information that is available in the literature alone. The most

important attribute of the force field is its the ability to predict the target properties with the desired accuracy. Another attribute is the type of the force field, i.e. the approach that is taken to model the atomistic architectures and their interactions. This is decisive for the computational cost but also relevant for the choice of the simulation tool, as not all programs can handle all types of force fields. Three different basic modeling levels are distinguished in the present work (cf. Fig. 1): all-atom (AA), united-atom (UA), and coarse-grained (CG) force fields.

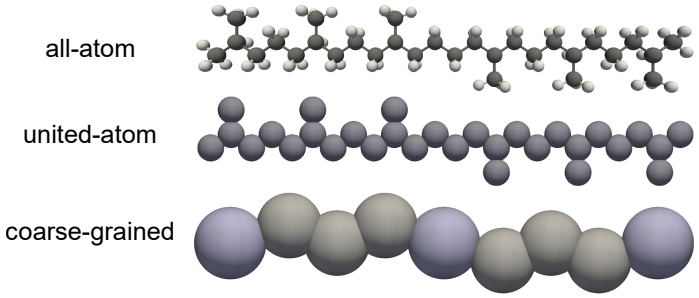

Figure 1: Sketch of a squalane molecule modeled by the different types of force fields.

In AA force fields, every atom is assigned to an individual interaction site. They are also often called 'explicit hydrogen' models. In contrast, UA force fields assign multiple atoms to a single interaction site. Usually, methylene and methyl groups are modeled by a single interaction site. The modeling by CG force field goes a step further and chain segments of multiple heavy atoms are combined to a single interaction site. For AA force fields, two subtypes can be further distinguished: (i) reactive AA force fields, which explicitly model chemical bonds (that can form and break during the simulation), and (ii) classical AA force fields, which are built using intramolecular potentials that do not break, e.g. a harmonic potential.

Nine force fields were applied in the present work for the modeling of five linear and branched alkanes, which are typical components of poly-α-olefines (PAO) or used as simple model lubricants. PAOs are an important group of lubricants.[39] The substances include the three linear alkanes n-decane ($C_{10}H_{22}$), n-icosane ($C_{20}H_{42}$), and n-triacontane ($C_{30}H_{62}$)

as well as two isomers of n-triacontane: 1-decene trimer and squalane (both $C_{30}H_{62}$). The chemical structures of the five substances investigated in this work are depicted in Fig. 2. In the following, the substances are abbreviated as n-C10, n-C20, n-C30, TRI, and SQU (cf. Fig. 2). Hence, the study comprises alkanes with different chain lengths as

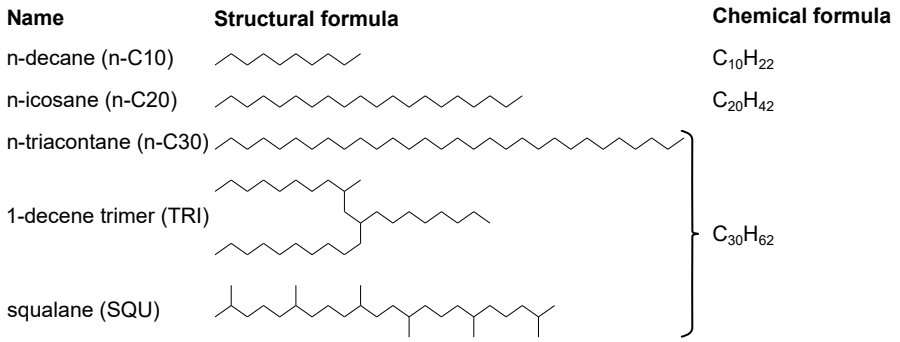

Figure 2: Overview of substances included in this study.

well as different structure for a given molecular formula. The molecule 1-decene trimer is the simplest (long branched) representative of poly-(1-decene) and it is an important component of PAO base oils.[39] Squalane (SQU) is frequently used as a model lubricant in experiments[29,40] and also an important substance in cosmetics.[41] The predictions for the density, the viscosity, and the self-diffusion coefficient of these substances were systematically compared to experimental data. Moreover, the computational costs of the different force fields were assessed. The study covers pressures up to 400 MPa, the temperature is always 373.15 K. The properties of lubricants at high pressure are of particular interest due to the high pressure conditions occurring in tribological applications.[2] Furthermore, the linear alkanes are common components of diesel fuels, whose properties at high pressure are also of high practical interest.[42]

Comparisons of different force fields have been published for a wide variety of substances. They address the prediction of phase equilibria[43,44] as well as bulk properties like the density,[25,26,37,45–48] isothermal compressibility,[37,44] and the speed of sound.[45] In some of the works, the ability of the force fields to predict thermophysical properties at elevated temperatures and pressures was explicitly addressed.[47,49,50] Studies explicitly addressing the

properties of lubricants are sparse. *Lin et al.* calculated the density and viscosity of a polyol ester (POE) lubricant at ambient pressure with three different force fields and compared them to experimental data.[48] *Ewen et al.* compared ten UA and AA force fields in their ability to predict the density and the viscosity of n-hexadecane up to 200 MPa.[26] The viscosity and the self-diffusion coefficient of branched alkanes as model lubricants have been studied by *Kondratyuk et al.*[25] A broad systematic comparison of force fields of different types regarding their ability to predict properties that are important for lubrication, i.e. density and viscosity, up to high pressures was, however, not available up to now. This gap is closed by the present study.

The different force fields lead to different computational costs of the molecular simulations. For example, the number of interaction sites per molecule varies for different force fields and has a strong influence. The computational costs normally scale linearly with the number of interaction sites for systems without electrostatic interactions.[51] With AA force fields, the number of interaction sites is approximately three times higher compared to UA force fields for alkanes. As CG force fields combine multiple UA sites to one site, the computational are further reduced. Another advantage of coarser modeling of the molecular structure consists of preventing high frequency oscillations (e.g. CH stretching bonds), which enables a larger time step. Furthermore, the type of interaction potentials to be evaluated strongly influences the computational costs, for example multibody or electrostatic interactions increase the computational time considerably.[52,53] Overall, multiple factors influence the computational cost of a simulation with a given force field and the costs can not be predicted a priori. Presently, no systematic comparison of the computational costs of different transferable force field types is available.

The following text is organized as follows: first, the methodology of the study is described which includes details of the conducted simulations, the sampling of the observables, information on the applied force fields, and the methods applied for the evaluation of the results. Then, the results for the three examined properties, the density, the viscosity, and

the self-diffusion coefficient, for all studied substances are presented and discussed. Thereafter, the computational costs of simulations with different force fields are compared. Finally, conclusions are drawn.

Methodology

Simulation details and evaluation

Equilibrium molecular dynamics simulations were carried out to calculate the density, the viscosity, and the self-diffusion coefficient of the studied pure substances. A cubic simulation box with periodic boundary conditions was used. The number of particles was chosen such that there were at least 200 molecules or 4000 interaction sites. The finite size dependency of the simulations was assessed by simulations with different numbers of molecules and extrapolating to the thermodynamic limit ($N_{\mathrm{mol}} \rightarrow \infty$). Details are given in the Supplementary Material. The results show that no significant finite size dependency applies to the results. The time step and integrator were chosen depending on the force fields and are summarized in Tab. 1. For the AA force field (excluding the reactive force fields), the RESPA multiple

Table 1: Time step and integrator used in the simulations.

force field type	time step / fs	integrator
AA	0.25 (bonds, angles), 0.5 (dihedrals), 1 (nonbonded)	RESPA[54]
AA (reactive)	0.25	
UA	0.5	Velocity-Verlet[55]
CG	10	

timestep method was used to reduce the computational costs. Thereby, the simulation time was reduced by a factor of at least 8 compared to the classical Velocity Verlet integrator with a time step of 0.25 fs. Details are given in the Supplementary Material. The cutoff radius was set to 14 Å throughout. An analytical long-range correction for the pressure was applied for the dispersive interactions.[55] Rigid bonds were realized using the SHAKE algorithm.[56] The electrostatic interactions were calculated by the particle-particle particle-mesh algorithm.[57]

All simulations were carried out with the LAMMPS package (Version 3 March 2020).[58] The initial configuration was built up by randomly inserting molecules into the box. For the reactive force fields, the molecules were inserted on a lattice to eliminate overlapping, which could lead to false molecule geometries as the geometry of the molecule is only given by the initial position. This insertion was done at a low density to avoid unphysical overlapping. Subsequently, the energy of the system was minimized by moving the particles to avoid large forces at the start of the MD simulations. After the energy minimization, the box volume was reduced to the target density within a short MD run of 100 ps. After this initialization phase, the actual simulations started.

For each substance and force field, five state points were studied. The pressures were $p \in \{0.1, 10, 100, 200, 400\}$ MPa and the temperature was $T = 373.15$ K in all cases. The density was determined by NpT simulations. The Nosé-Hoover thermostat and barostat[59–61] were used to control the temperature and the pressure in the simulations. The damping times comprised 100 timesteps for the thermostat and 1000 timesteps for the barostat, as recommended in the LAMMPS documentation.[58] Each NpT simulation had an equilibration time of 1 ns and a production time of 2 ns. To ensure that the simulation is sufficiently long enough, longer simulations have been run. More details are given in the Supplementary Material. To reduce the statistical uncertainty, each NpT simulation was replicated five times and the density of each state point was calculated as the average of these five replica simulations. This density was then taken as input for NVT simulations to determine the viscosity and the self-diffusion coefficient. To calculate the transport properties, 20 independent NVT simulations were carried out for each state point. The equilibration time was 1 ns. The production time varied from 2 to 10 ns and was determined individually for each state point and substance, and was chosen to obtain convergence of the correlation functions. Details are summarized in Tab. 2.

Table 2: Simulation times in ns for the different substances and state points.

	substance		
p/MPa	n-C10	n-C20	n-C30, TRI, SQU
0.1	2	3	4
10	2	3	4
100	2	4	6
200	2	6	8
400	4	6	10

The viscosity was calculated using the Green-Kubo relations[62,63] given by

$$\eta(\tau) = \frac{1}{V k_\mathrm{B} T} \int_0^{\tau \to \infty} \left\langle J_\mathrm{p}^{\alpha\beta}(t+\tilde{\tau}) \cdot J_\mathrm{p}^{\alpha\beta}(t) \right\rangle \mathrm{d}\tilde{\tau} \,, \tag{1}$$

where V is the box volume, k_B the Boltzmann constant, T the temperature, t the reference time, τ the time variable, and $J_\mathrm{p}^{\alpha\beta}$ the non-diagonal entries of the stress tensor.[55] The pressure tensor was sampled every 4 fs during the NVT simulations. Each of the sampled time steps was taken as reference time t to achieve best possible statistics. The time decomposition method (TDM)[33] was applied in this work, which enables the reliable calculation of high viscosities by EMD simulations. Therefore, the viscosity time evolution $\eta(\tau)$ was calculated for all 20 NVT simulations during the production run. For the calculation of the ACF, a fast Fourier transform (FFT) technique was used.[64] Contributions from all six independent entries of the pressure tensor $p_{\alpha\beta}$ were averaged to calculate the viscosity as proposed by Ref.[65] The cutoff time τ_cut for the ACFs (to circumvent the ACF long-term noise) were determined from the standard deviations $\sigma_\eta(\tau)$ as $\frac{\sigma_\eta(\tau_\mathrm{cut})}{\eta(\tau_\mathrm{cut})} = 0.4$ as recommended in Ref.[33] Different numbers $\frac{\sigma_\eta(\tau_\mathrm{cut})}{\eta(\tau_\mathrm{cut})}$ for the cutoff time have been compared in the Supplementary Material. The bootstrapping method[33] with 200 iterations was used to calculate the final value and its uncertainty for the viscosity. Therefore, 200 combinations of the 20 simulations were created randomly whereas multiple appearances of individual simulations were allowed. For each combination, an average viscosity $\bar{\eta}(\tau)$ was calculated and the function given in

Eq. (2) was fitted to $\bar{\eta}(\tau)$ where η_∞ is the long term limit.

$$\eta(\tau) = \eta_\infty \frac{\alpha\beta_1\left(1 - e^{-\frac{\tau}{\beta_1}}\right) + (1-\alpha)\beta_2\left(1 - e^{-\frac{\tau}{\beta_2}}\right)}{\alpha\beta_1 + (1-\alpha)\beta_2} \tag{2}$$

Fig. 3 illustrates the TDM method for two state points showing the viscosity sampled during the production phase $\eta(\tau)$. The results for all 20 simulation replica are shown. The

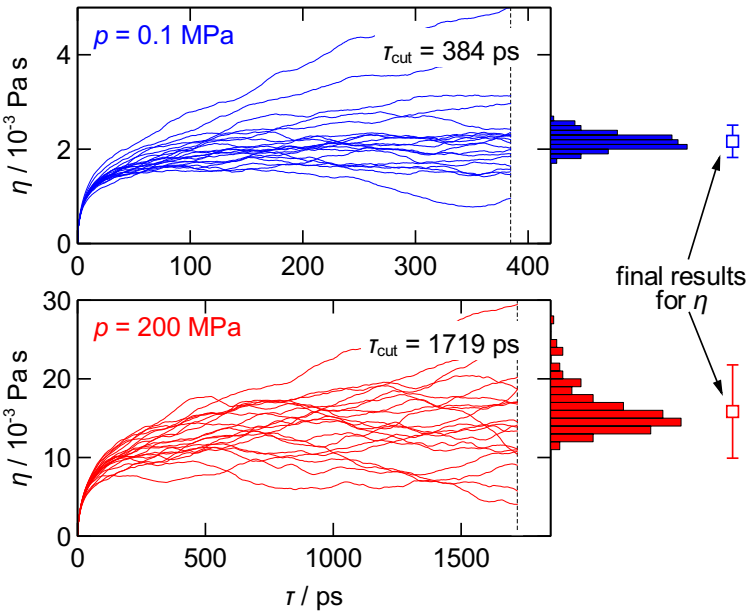

Figure 3: Illustration of the TDM method. Results for the sampled viscosity from 20 independent runs $\eta(\tau)$ over time τ of TRI at p = 0.1 MPa (top) and p = 200 MPa (bottom) (T = 373.15 K for both). Histograms of the corresponding bootstrapping results and the final result of the bootstrapping method.

two simulations have different cutoff times τ_{cut}, which compensates differences of long-term noise behavior. On the right-hand side of Fig. 3, also the final values and the histograms consisting of 200 η_∞ values as obtained from the bootstrapping method are shown. The statistical uncertainties were computed from the histogram as the 95 % confidence interval. The individual results for $\eta(\tau)$ show in parts a wide scattering that increases with time, which is a well-known phenomenon.[66] The time required to reach a stable plateau of the viscosity differs strongly which can also be seen by the different cutoff times. Overall, the TDM method provides relatively low statistical uncertainties and enables a reliable calculation of

the viscosity.

The self-diffusion coefficient D was calculated by the Einstein relation[55]

$$D = \lim_{\tau\to\infty} \frac{\mathrm{d}}{\mathrm{d}\tau} \frac{1}{6} \left\langle \frac{1}{N} \sum_{i=1}^{N} \left| \boldsymbol{r}_i(t+\tau) - \boldsymbol{r}_i(t) \right|^2 \right\rangle , \tag{3}$$

where N is the number of particles in the box and $\boldsymbol{r}_i$ is the position vector of center of mass of the molecule or particle i. A calculation of the self-diffusion coefficient by the Green-Kubo relation and the TDM method was not feasible as it would require to write out the velocity vector of all atoms with a high frequency. The Einstein relation requires the positional data of all atoms less frequently. In this work, the positional data were written out every 10 ps. The term $\left| \boldsymbol{r}_i(t+\tau) - \boldsymbol{r}_i(t) \right|^2$ is the mean square displacement (MSD). It is possible to calculate the MSD either from the atomic or the molecular center of mass.[67] In this work, the molecular center of mass was used. The MSD was calculated by making use of the FFT method.[64] The self-diffusion coefficient D was calculated individually for each NVT simulation using Eq. (3). By averaging the results of the 20 independent simulations, a single value for D was obtained for every state point. The statistical uncertainty of D was calculated as the standard error as

$$\Delta D = \sqrt{\frac{1}{N_\mathrm{rep}} \sum_{i=1}^{N_\mathrm{rep}} (D_i - D)^2} , \tag{4}$$

with $N_\mathrm{rep} = 20$. The self-diffusion is subject to finite size effects that are not negligible.[68] There are two methods to obtain the self-diffusion coefficient in the thermodynamic limit (i.e. infinite box size). The classical brute force approach is conducting multiple simulations with different box sizes and extrapolating to the thermodynamic limit. This is not feasible in this work since a large number of state points and force fields are studied. Instead, the

analytical correction term proposed by *Yeh and Hummer*[69] was applied as

$$D_{L\to\infty} = D(L) + \frac{k_\mathrm{B}T\xi}{6\pi\eta L}\,, \tag{5}$$

where L is the box length of the simulation, η the viscosity, and $\xi = 2.837297$ is a dimensionless constant (adopted from Ref.[69]).

Force fields

Tab. 3 gives an overview of the force fields studied in this work and their assignment to force field classes. All force field parameters used in this study and validations of the implementations are given in the Supplementary Material.

Table 3: Overview of all force fields used in this work.

name	type	refs.	published
OPLS	AA	[70]	1996
COMPASS	AA	[71]	1998
L-OPLS	AA	[72]	2012
ReaxFF	AA (reactive)	[73]	2001
AIREBO-M	AA (reactive)	[74]	2015
TraPPE	UA	[75,76]	1998
Potoff	UA	[77,78]	2009
TAMie	UA	[79,80]	2015
MARTINI	CG	[81]	2007

All-atom force fields (AA)

In this study, the AA force fields COMPASS,[71] OPLS,[70] L-OPLS,[72] ReaxFF,[82] and AIREBO-M[74,83] were used. The latter two force fields are so-called reactive all-atom force fields that allow bond breaking. However, no bond breaking was observed in the simulations carried out in this work, hence, no special distinctions from the other all-atom force fields are necessary here. All AA force fields except AIREBO-M include Coulomb interactions. The COMPASS force field models the dispersive interactions by a 9-6 Mie potential. The intramolecular

interactions include bonds, angles, dihedrals, impropers as well as cross terms, which include mixed bond, angle, and dihedral contributions. The parameters of the COMPASS force field were determined from a fit to quantum-mechanical (QM) data (charges and intramolecular potentials) and to liquid state properties (dispersive potential).[71] In the OPLS force field, the classical Lennard-Jones (LJ) 12-6 potential is used for modeling the dispersive interactions. The bond and angle parameters of the OPLS force field were adopted from the CHARMM/22 force field.[70,84] The torsional and the dispersive parameters were fitted to QM data and different thermodynamic and structural properties, respectively. The L-OPLS force field adopts the majority of the OPLS parameters but dihedral and dispersive parameters as well as the charges were refined to improve the modeling of longer hydrocarbons.[72] Additionally, the bonds between carbon and hydrogen were constrained to a constant distance in the L-OPLS force field. It is known that the L-OPLS provides better predictions for bulk properties compared to the OPLS force field.[26] As the OPLS force field is still widely used in its original version, it was also included in this study.

The ReaxFF[82] and AIREBO-M[74,83] force fields include explicit calculations of the bond order, which enables them to model chemical reactions.[52] The *CHON-2017_weak* version of the ReaxFF force field[73] was implemented in this work. It includes parameter adjustments that aim at improving the density prediction of the condensed phase.[73] The AIREBO-M force field[74] was derived from the AIREBO force field[83] by replacing the LJ potential interactions by a Morse potential. Its parameters were adjusted to layer spacing of graphite up to pressures of 14 GPa and to QM data of small alkanes. Both reactive force fields were only applied to n-decane (n-C10) in the present work due to their extremely high computational costs.

United-atom force fields (UA)

The TraPPE,[75] Potoff,[77] and TAMie[79] UA force fields were used in this study. The TraPPE force field uses the classical 12-6 LJ potential. These LJ parameters were fitted to critical

temperatures and saturated liquid densities. The Potoff and the TAMie force fields use n-6 Mie potentials for the non-bonded interactions. In both force fields, the repulsive parameter n of the Mie potential was additionally adjusted in the fitting procedure. For the TAMie and the Potoff force fields, the non-bonded parameters were fitted to saturated liquid densities and vapor pressures. The cutoff distance of the Potoff force field was set to 10 Å as recommended.[77] In contrast to the AA force fields, there are no Coulomb interactions for UA models of hydrocarbons as all interaction sites are electrostatically neutral. In this work, flexible bonds between the interaction sites were applied. Therefore, a harmonic potential was used with the given bond length as equilibrium bond length. The energy parameter of the bond potential was taken from the OPLS force field. Despite the fact that the TraPPE, Potoff, and TAMie force fields were originally developed using rigid bond lengths, it is common practice to adapt them with flexible bonds.[85–87] Moreover, it was shown that the flexible bonds do not influence the results if the bond force constant is well chosen.[49,88] The angle and dihedral potentials are the same for all three UA force fields as they were mainly adopted from the OPLS-UA[89] and OPLS-AA[70] force fields.

Coarse grained force field (CG)

In this study, the MARTINI CG force field was used. There are two approaches to parameterize CG force fields: bottom-up by derivation from a finer resolved force field (e.g. AA) and top-down by fitting parameters directly to experimental data.[90] The MARTINI force field[81] is based on the top-down approach. It was parameterized to the free energy of hydration and vaporization as well as the partitioning free energies between water and multiple organic substances.[81] A four-to-one mapping is applied by the MARTINI force field in general, which means four heavy atoms (all atoms except hydrogen atoms) are fused to a single interaction site. The force field consists of the LJ potential for non-bonded parameters and harmonic potentials for the angle and bond interactions. There are no dihedral potentials. The mapping of molecules to CG beads is not strictly defined. There are several methods to

create CG models from a given molecular topology.[91–93] In this study, the automatic mapping algorithm from *Potter et al.*[93] was applied. As the mapping may in general have an influence on the force field predictions, the MARTINI results should be considered as results obtained from "MARTINI + Potter mapping". For brevity, only "MARTINI" is used in the following. The bond lengths of the created models were adjusted as suggested in Ref.[93] for the prediction of thermodynamic bulk properties. The MARTINI 2[81] version was used in this work instead of the recently published MARTINI 3 force field[94] as the MARTINI 2 version has been widely applied in recent years – and as different auxiliary tools are available for MARTINI 2.

Data analysis

The simulation results for the density, the viscosity, and the self-diffusion coefficient were analyzed in a consistent way as described in the following. As a basis, correlations to all available experimental literature data were developed. An overview of the available data for the five considered substances and the three considered thermophysical properties is given in Tab. 4. The functions, parameters, and accuracy of the correlations are reported in the

Table 4: Overview of available experimental literature data (references given) and the corresponding maximum pressures for the different substances and properties examined in the current study. "n.a." indicates that no literature data were found.

	n-C10		n-C20		n-C30		TRI		SQU	
	Ref.	$\frac{p_{max}}{MPa}$	Ref.	$\frac{p_{max}}{MPa}$	Ref.	$\frac{p_{max}}{MPa}$	Ref.	$\frac{p_{max}}{MPa}$	Ref.	$\frac{p_{max}}{MPa}$
ρ	[95–98]	279	[99,100]	500	[99]	500	n.a.		[40,101–104]	243
η	[96,105]	300	[106]	243	n.a.		[35]	1298	[35,107]	1298
D	[108]	200	n.a.		[109]	600	n.a.		n.a.	

Supplementary Material. They represent the experimental data within relative deviations of up to 0.3 % (ρ), 5.2 % (η), and 2.6 % (D). Furthermore, also correlations for the properties where no experimental data was available are provided in the Supplementary Material. These correlations were created on the basis of the simulation data of the Potoff force field (which turns out to be clearly the most accurate force field among those studied here). Their

parameters are also reported in the Supplementary Material. For the assessment of the force fields with respect to the experimental data, the deviations of the simulation results to the correlations of the experimental data were calculated from

$$\delta Y_{\mathrm{exp}} = \frac{Y_{\mathrm{sim}} - Y_{\mathrm{corr}}}{Y_{\mathrm{corr}}} \quad \text{for} \quad Y \in \{\rho, \eta, D\}. \tag{6}$$

The total average deviation $\overline{\delta Y}$ of a force field was calculated as the mean value of $|\delta Y_{\mathrm{exp}}|$ ($Y \in \{\rho, \eta, D\}$) averaged over all state points and substances for which experimental data were available (cf. Tab. 4).

Results

In the following, the simulation results for the density ρ, the viscosity η, and the self-diffusion coefficient D are presented and discussed. Where available, also the experimental data is included in the discussion. Furthermore, correlations of the experimental data (cf. Section) are shown and used as a reference for the deviation plots. Where no experimental data were available, a correlation of the simulation data of the Potoff force field were used as a reference. The numeric data of all simulations shown are given in the electronic Supplementary Material. Fig. 4 shows three snapshots of different n-decane (n-C10) simulations, one for each force field type. It illustrates the different abstraction levels at which the molecules were modeled by the different force field types. The structure of the molecules was evaluated by the radius of gyration. Details are given in the Supplementary Material.

Fig. 5 gives an overview of the total average deviations $\overline{\delta Y}$ of all force fields for the three studied properties, the density, the viscosity, and the self-diffusion coefficient ($Y \in \{\rho, \eta, D\}$). The total deviations are lowest for the density with up to $\overline{\delta\rho} = 6.4$ %. The deviations for the viscosity and the self-diffusion are substantially larger (up to $\overline{\delta\eta} = 210.1$ % and $\overline{\delta D} = 70$ %). For a given force field, the deviations of the viscosity and self-diffusion predictions are very similar for most force fields. As can be seen from Fig. 5, there is no direct indication that the

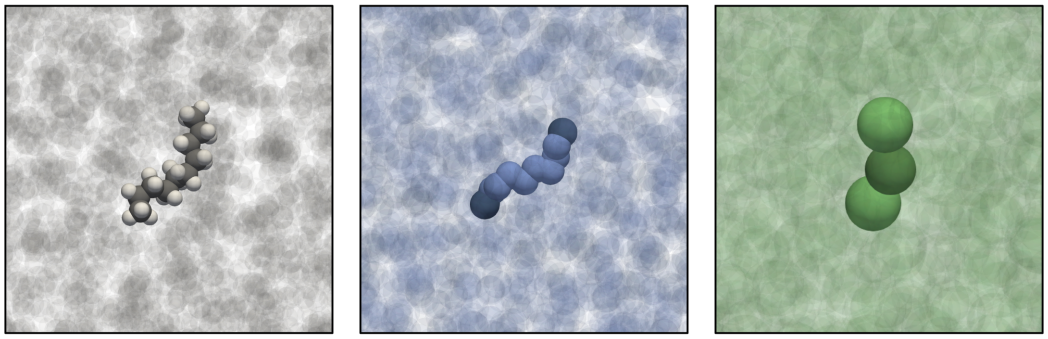

Figure 4: Snapshots of three n-decane simulations (p = 0.1 MPa). The force fields are: (a) L-OPLS (AA), (b) TraPPE (UA), and (c) MARTINI (CG). The length scale is the same for all snapshots. One molecules is highlighted in each snapshot. The single sites are colored as follows: light green - end site of the CG model, dark green - central site of the CG model, light blue - CH_2, dark blue - CH_3, gray - carbon, white - hydrogen.

deviation depends on the force field type as the deviations scatter also within the different force field types (AA, UA, and CG). This indicates that the individual parametrization of a force field (cf. Section) is more important for the deviations produced by the force field. The total average deviations of the single force fields are discussed in detail in the following sections.

Density

The simulation results for the density are shown in Fig. 6 in comparison to experimental data (where available). The corresponding deviation plots are shown in Fig. 7.

The Potoff UA force field gives excellent predictions of the density, the average deviation from the experimental data $\overline{\delta\rho}$ is only 0.4 %. The predictions obtained with the TAMie UA force field are also good ($\overline{\delta\rho}$ = 1.3 %). The third studied UA force field, TraPPE, yields poorer results ($\overline{\delta\rho}$ = 2.4 %). The TraPPE force field tends to overestimate the density, especially for the linear alkanes.

Despite their higher complexity, the AA force fields OPLS, L-OPLS, and COMPASS generally do not yield better results than the UA force fields. Among the AA force fields,

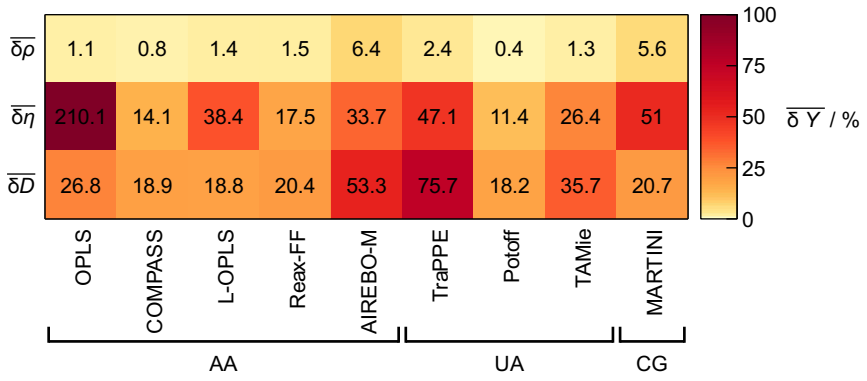

Figure 5: Total average deviations of the simulation results to the correlations of experimental data (values given in %) for the density $\overline{\delta\rho}$, the viscosity $\overline{\delta\eta}$, and the self-diffusion coefficient $\overline{\delta D}$.

COMPASS ($\overline{\delta\rho}$ = 0.8 %) is slightly better than the two others (OPLS: $\overline{\delta\rho}$ = 1.1 %, L-OPLS: $\overline{\delta\rho}$ = 1.4 %). In assessing the results from the OPLS force field, it has to be considered that it predicts n-C20 and n-C30 to be solid for the conditions studied here. This is in line with findings from the literature,[110] which report that the OPLS force field predicts the liquid-solid phase transition for long alkanes at temperatures that are much higher than the experimental melting temperature.[72] More details on this are given in the Supplementary Material. The OPLS data for n-C20 and n-C30 are excluded for the present discussion.

The reactive AA force fields ReaxFF and AIREBO-M were only applied to n-C10. ReaxFF ($\overline{\delta\rho}$ = 1.5 %) overestimates the density, AIREBO-M ($\overline{\delta\rho}$ = 6.4 %) strongly underestimates it, cf. Fig. 7. The latter yields the poorest prediction of the density. The CG force field MARTINI ($\overline{\delta\rho}$ = 5.9 %) also shows high deviations.

The pressure dependency of the density $(\mathrm{d}\rho/\mathrm{d}p)_T$ is predicted generally quite well by most of the models (cf. Fig. 6). Among the UA force fields, the TraPPE force field yields the poorest prediction of the pressure dependency of the density as it overestimates $(\mathrm{d}\rho/\mathrm{d}p)_T$. While the Potoff force field slightly underestimates $(\mathrm{d}\rho/\mathrm{d}p)_T$, the results obtained from the TAMie force field do not show this tendency. This difference originates from the different repulsive Mie coefficients n of the TraPPE (n = 12), the TAMie (n = 14), and the Potoff (n = 16) force fields. The higher the repulsive coefficient, the lower is $(\mathrm{d}\rho/\mathrm{d}p)_T$. This

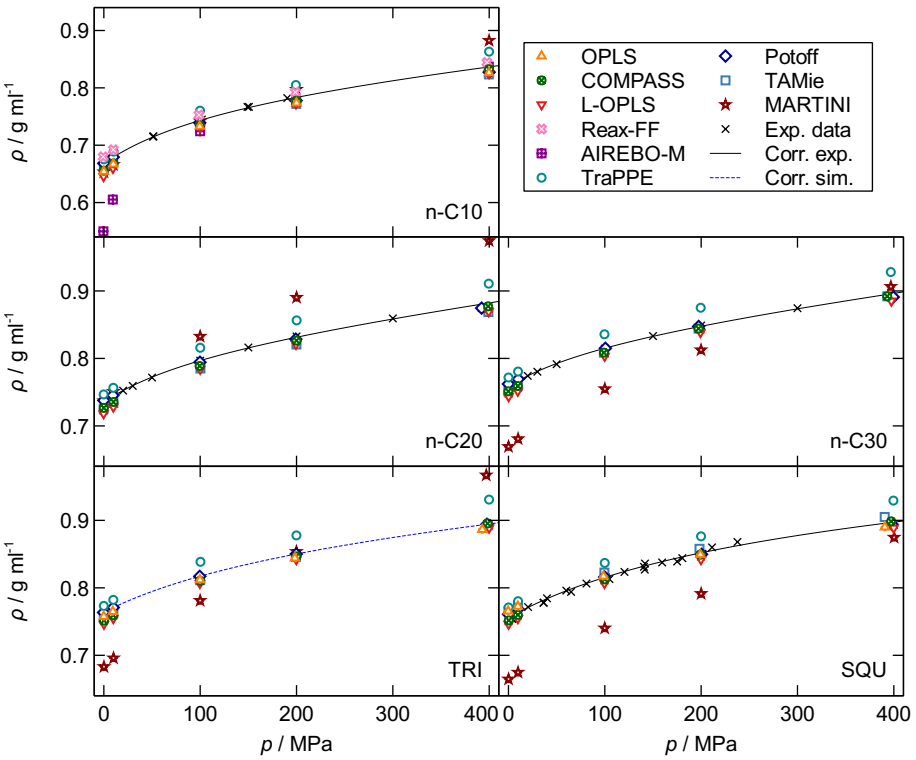

Figure 6: Density ρ of n-C10, n-C20, n-C30, TRI, and SQU at T = 373.15 K as a function of the pressure p. Colored symbols indicate the simulation results for the different force fields and the black crosses are experimental data points (cf. Tab. 4). Black solid lines are correlations of the experimental data, blue broken lines are correlations of the simulation data with the Potoff force field.

also holds for the three classical AA force fields, which also utilize a Mie potential (OPLS: n = 12, COMPASS: n = 9, L-OPLS: n = 12) and overestimate $(\mathrm{d}\rho/\mathrm{d}p)_T$. Besides the potential, also the choice of the state points used for parametrization influences the results. This can especially be seen for the AIREBO-M force field, which was fitted including state points at high pressure. Its predictions of the density are best for the highest investigated pressure (400 MPa).

Viscosity

The results for the viscosity are shown in Fig. 8 using a logarithmic scale as a function of pressure. The corresponding deviation plots are shown in Fig. 9. Again, the results for n-C20 and n-C30 obtained with OPLS are discarded from the discussion as they refer to

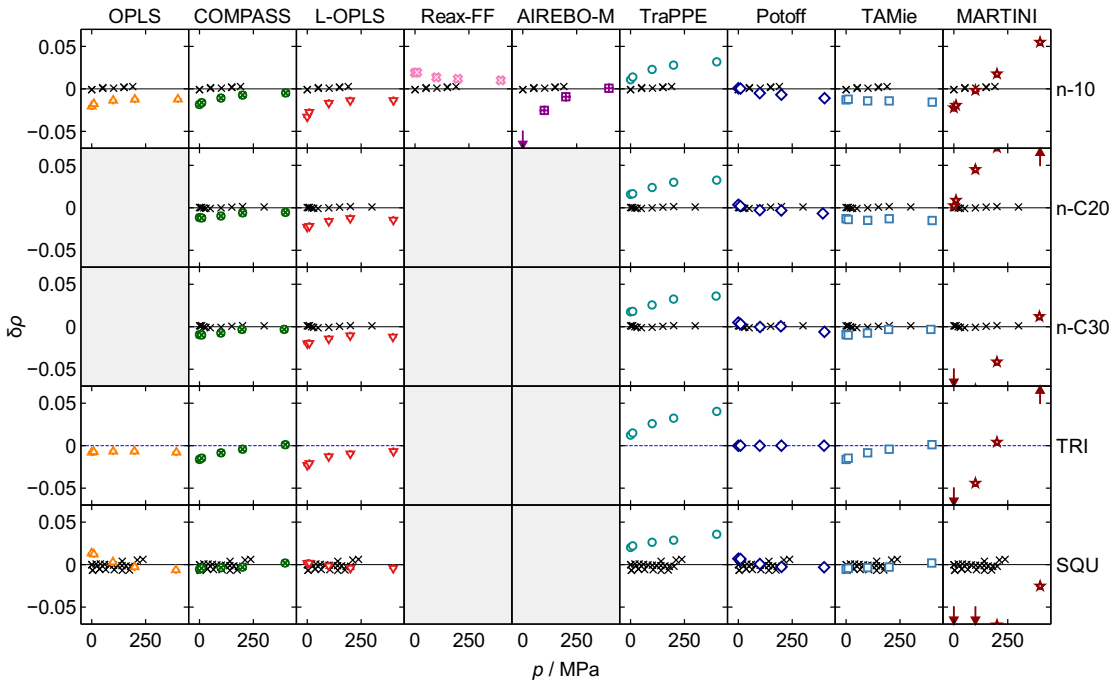

Figure 7: Relative deviation of the density $\delta\rho$ (cf. Eq. (6)) at T = 373.15 K as a function of the pressure p for all studied force fields and substances. The relative deviation (cf. Eq. (6)) refers to the correlation, which was obtained from either experimental data (black crosses, cf. Tab. 4) or the simulation data with the Potoff force field (dark blue diamonds).

solids (cf. Supplementary Material). As expected, the viscosity of all substances increases approximately exponentially with increasing pressure. Moreover, the viscosity of the linear alkanes (n-C10 to n-C30) increases with increasing chain length. This behavior is described well by all studied force fields. In contrast to the predictions of the density, the scattering of the results is larger and the predictions from the different force fields deviate in a range of an order of magnitude. This scattering is larger for the two branched alkanes (TRI, SQU) compared to the linear alkanes (n-C10 to n-C30).

As already seen for the density results, the Potoff UA force field gives the best predictions for the viscosity with $\overline{\delta\eta}$ = 11.4 %. The deviations obtained with the TAMie UA force field are doubled ($\overline{\delta\eta}$ = 26.4 %) compared to the Potoff UA force field and show an underestimation of the viscosity, especially for high pressures. *Messerly et al.*[49] found similar deviations for the Potoff and TAMie force fields for the viscosity of shorter alkanes. The TraPPE UA

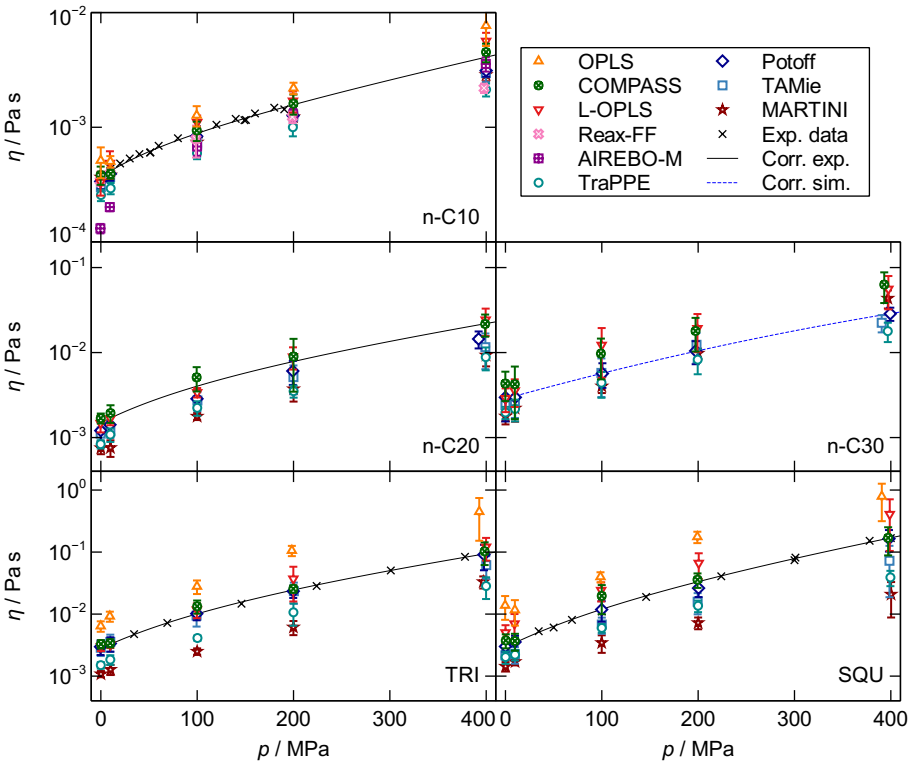

Figure 8: Viscosity η of n-C10, n-C20, n-C30, TRI, and SQU at T = 373.15 K as a function of the pressure p. Colored symbols indicate the simulation results for the different force fields and the black crosses are experimental data points (cf. Tab. 4). Black solid lines are correlations of the experimental data, blue broken lines are correlations of the simulation data with the Potoff force field.

force field strongly underestimates the viscosity and yields the largest deviations from the experimental data among the UA force fields ($\overline{\delta\eta}$ = 47.1 %). The underestimation of the viscosity by the TraPPE force field was already stated in literature.[45,49,111] The only CG force field, MARTINI, has similar deviations from the experimental correlations with $\overline{\delta\eta}$ = 51 %, which is in accordance with results reported in literature.[47] The time scale, which is crucial for the calculation of the viscosity (cf. Section), is often scaled in CG simulations as CG models usually exhibit faster dynamics compared to higher resolution atomistic models. Therefore, a time scaling factor of 4 is often applied.[81] In the Supplementary Material, results for the viscosity calculated by the MARTINI force field are given with a time scaling factor of 4. For the three linear alkanes, the results do not improve compared to the results without conversion factor. The scaled results overestimate the experimental values. For the

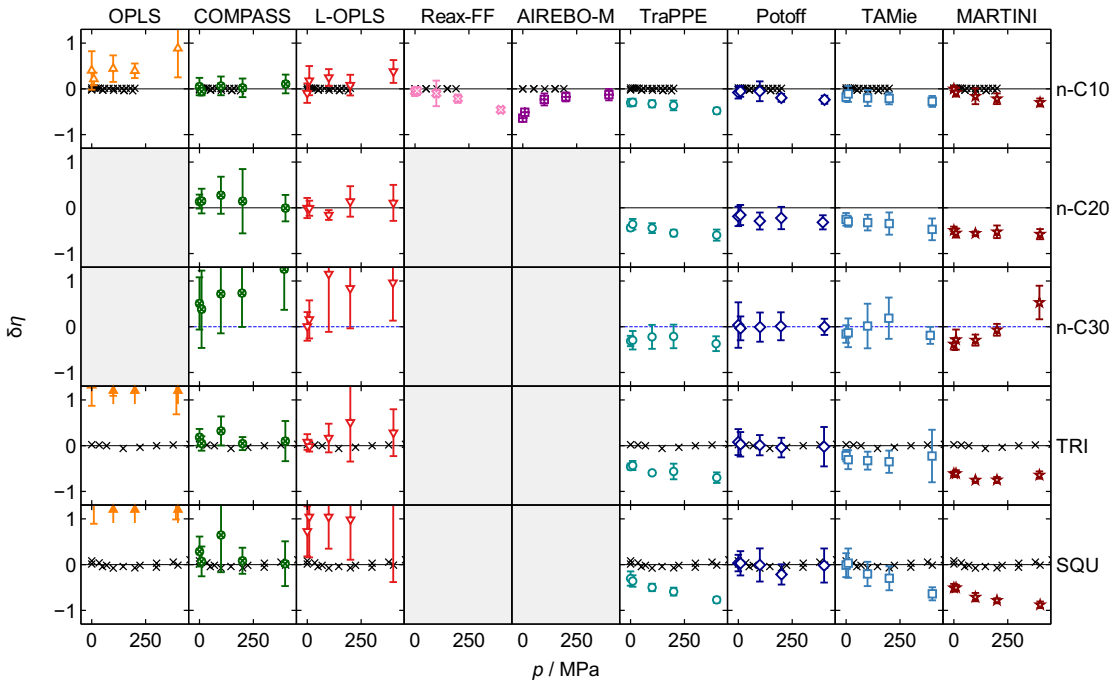

Figure 9: Relative deviation of the viscosity $\delta\eta$ (cf. Eq. (6)) at T = 373.15 K as a function of the pressure p for all studied force fields and substances. The relative deviation (cf. Eq. (6)) refers to the correlation, which was obtained from either experimental data (black crosses, cf. Tab. 4) or the simulation data with the Potoff force field (dark blue diamonds).

two branched alkanes, the scaling improves the results and decreases the deviations to the experimental data. More details are given in the Supplementary Material. Yet, in the main body of this work, results without a scaling factor are presented.

The AA force fields show very different behaviors. The COMPASS ($\overline{\delta\eta}$ = 14.1 %) and the ReaxFF ($\overline{\delta\eta}$ = 17.5 %) force fields yield good predictions for the viscosity. The latter predicts the viscosity accurately up to a pressure of around 100 MPa which is in accordance with findings reported by *Morrow and Harrison*[37] for alkanes and other thermophysical properties. For higher pressure, the viscosity is underestimated by the ReaxFF force field. For the COMPASS force field, there is a tendency for overestimation of the viscosity predicted (which has also been reported by Refs.[8,25]). The AIREBO-M force field predicts the viscosity with $\overline{\delta\eta}$ = 33.7 %. Its deviations decrease with increasing pressure. The L-OPLS force field deviates with $\overline{\delta\eta}$ = 38.4 % from the experimental data on average. Thus, it shows a good

improvement to the closely related OPLS force field,[26,112] which yields by far the worst predictions for the viscosity ($\overline{\delta\eta}$ = 210.1 %). The poor prediction ability of the viscosity by the OPLS force field was already reported for shorter alkanes.[25,111,112] In general, the AA force fields have larger error bars compared to the UA and CG force fields, especially for the large molecules n-C30, TRI, and SQU.

Self-diffusion coefficient

The results for the self-diffusion coefficient using a logarithmic scale as function of pressure and the corresponding deviation plot are shown in Fig. 10 and 11, respectively. Here, also

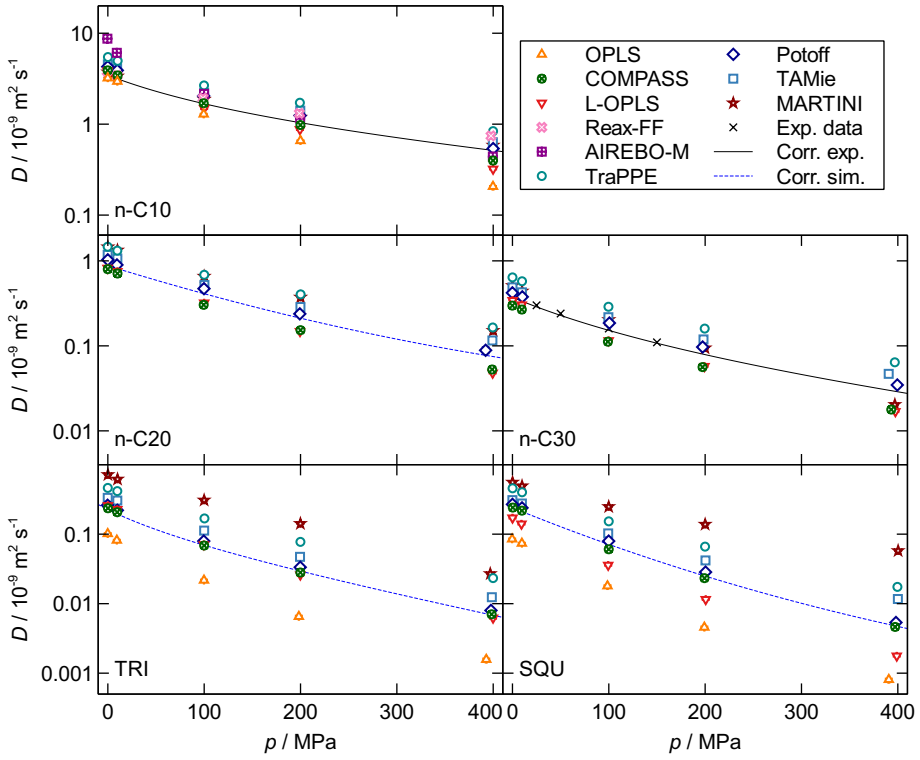

Figure 10: Self-diffusion coefficient D of n-C10, n-C20, n-C30, TRI, and SQU at T = 373.15 K as a function of the pressure p. Colored symbols indicate the simulation results for the different force fields and the black crosses are experimental data points (cf. Tab. 4). Black solid lines are correlations of the experimental data, blue broken lines are correlations of the simulation data with the Potoff force field.

the results of the OPLS force field for n-C20 and n-C30 are discarded and can be found in the Supplementary Material. The self-diffusion coefficient decreases with increasing pressure

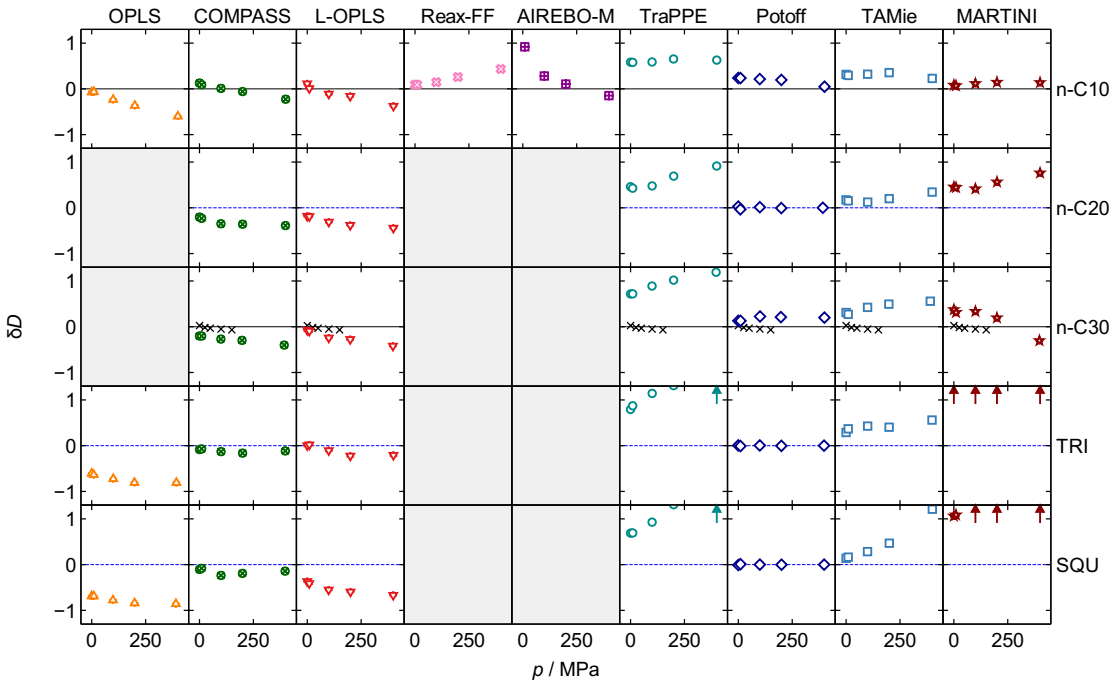

Figure 11: Relative deviation of the self-diffusion coefficient δD (cf. Eq. (6)) at T = 373.15 K as a function of the pressure p for all studied force fields and substances. The relative deviation (cf. Eq. (6)) refers to the correlation, which was obtained from either experimental data (black crosses, cf. Tab. 4) or the simulation data with the Potoff force field (dark blue diamonds).

for all substances and force fields – as expected. The close relation of the self-diffusion coefficient and the viscosity[113] can be observed in the MD simulation results: high values for the viscosity go along with low values for the self-diffusion and vice versa. Therefore, the self-diffusion coefficient shows opposite characteristics compared to the viscosity (cf. Section) regarding the deviations of the single force fields. In the Supplementary Material, figures of the viscosity plotted as a function of the self-diffusion coefficient are shown to underline their close relation.

The predictions for the self-diffusion coefficient with the Potoff force field are again the best and show the lowest deviations from the experimental data with $\overline{\delta D}$ = 18.2%. This is in line with the results for the density and the viscosity. The TAMie force field overestimates the self-diffusion for all substances with a total deviations of $\overline{\delta D}$ = 35.7%. The TraPPE force field also predicts too high values for the self-diffusion coefficient but with a much higher total

deviation ($\overline{\delta D}$ = 75.7%). For both the TAMie and the TraPPE force fields, the deviations increase with increasing pressure. The MARTINI CG force field predicts the self-diffusion coefficient surprisingly well with a total deviation of $\overline{\delta D}$ = 20.7%. Like the viscosity, the self-diffusion coefficient is a time-dependent property and thus, it is also influenced by time scaling, as often applied in CG simulations. As for the viscosity, results with time scaling are given for the self-diffusion coefficient in the Supplementary Material. The results are similar to those for the viscosity: For the linear alkanes, results worsen compared to experimental values and the self-diffusion coefficient is underestimated. For the two branched alkanes, the predictions improve compared to the experimental data. More details are given in the Supplementary Material. In the main part of this work, results without a scaling factor are presented.

The COMPASS ($\overline{\delta D}$ = 18.9%) and the L-OPLS ($\overline{\delta D}$ = 18.8%) force fields exhibit nearly the same total deviations. Their predictions are very good and similar to those of the Potoff force field. With $\overline{\delta D}$ = 20.4%, also the ReaxFF force field shows good predictions for the self-diffusion coefficient. They both slightly overestimate the self-diffusion coefficient. The OPLS force field also overestimates the self-diffusion coefficient with a total deviation of $\overline{\delta D}$ = 26.8%. This was already reported in literature for simulations of n-hexane with the OPLS force field.[114] The deviations of the OPLS force field are much lower for the self-diffusion compared to the viscosity as only n-C10 is included in the calculation of the total deviation. The AIREBO-M force field shows the second largest total deviations ($\overline{\delta D}$ = 53.3%) for the self-diffusion coefficient.

Computational costs

The computational costs of the different force fields were evaluated by additional simulations for n-C10 at one state point (T = 373.15 K and ρ = 0.67982 g/ml). 20 replica simulations were conducted for each force field and the viscosity and the self-diffusion coefficient were calculated as described in Section . As the density strongly influences the computational

costs, the same density was prescribed to the simulations for all force fields. All simulations for the determination of the computational costs were executed on the same machine with *Intel XEON SP 6126* processors and with the same simulation parameters (200 molecules, 1 ns equilibration, 2 ns production run, cutoff radius of 14 Å). Different number of cores have been used for the different simulations (AA: 24 cores, UA: 8 cores, CG: 1 core) to ensure perfect parallel efficiency. The computational costs were measured using the CPU hours (*cpuh*), i.e. *cpuh* = *number of processors* × *simulation time* required for a given simulation. The results for the computational costs are shown in Fig. 12. The computational costs are normalized with respect to the OPLS force field computational costs. The statistical

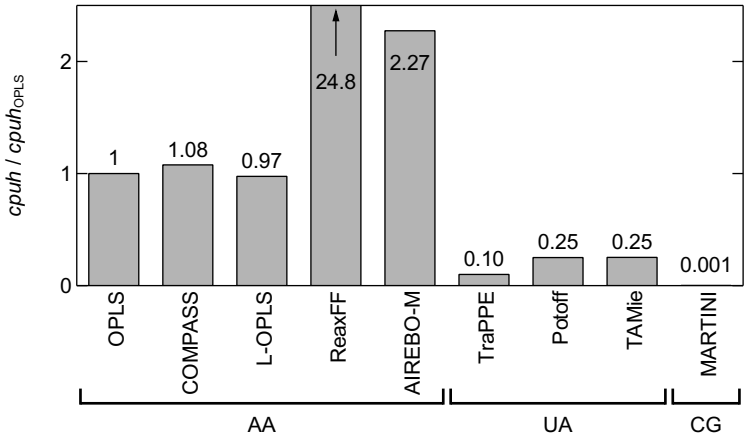

Figure 12: Computational costs *cpuh* of all force fields normalized with respect to the computational costs of the OPLS force field $cpuh_{\mathrm{OPLS}}$ for 20 replica simulations with $T = 373.15\,\mathrm{K}$ and $\rho = 0.67982\,\mathrm{g/ml}$.

uncertainties obtained from these simulations are reported in the Supplementary Material.

The three classical AA force fields, OPLS, COMPASS, and L-OPLS, require similar computational costs, as expected. The slightly increased computational costs of the COMPASS force field compared to the OPLS and the L-OPLS force field are due to the use of more complex functions for computing the interactions in the COMPASS force field (including cross terms, e.g. bond-angle interactions). The two reactive AA force fields, ReaxFF and AIREBO-M, require substantially higher computational costs. The ReaxFF force field requires by far the highest costs with approximately 25 times the costs of the classical AA

force fields.

The three UA force fields require lower computational costs than the AA force fields with 10 % - 25 % of the costs of the AA force fields. For studying the computational costs, the cutoff radius of the Potoff force field was set to 14 Å (equal to the other force fields). The higher computational costs of the Potoff and the TAMie force fields compared to the TraPPE force field are due to the use of the Mie potential instead of the 12-6 LJ potential. The latter is computationally more efficient as the repulsive part (exponent n = 12) and the attractive part (exponent m = 6) can be evaluated simultaneously benefiting from $r^{12} = \left(r^6\right)^2$. Furthermore, the calculation of the mixed exponent for Mie parameters produces an additional computational overhead. The low computational costs of the MARTINI CG force field are due to the small number of interaction sites and the larger time step used in the MARTINI simulations.

The uncertainties of the simulations are given in the Supplementary Material. The statistical uncertainties for the viscosity are about an order of magnitude larger compared to the self-diffusion coefficient results. For a given property, the different force fields yield similar statistical uncertainties.

Conclusions

The ability of different force fields to predict the density, the viscosity, and the self-diffusion coefficient of model lubricants was investigated. Pure linear (n-decane, n-icosane, n-triacontane) and branched alkanes (1-decene trimer, squalane) up to C30 were studied. The results were compared to experimental data where such data were available. The force fields consisted of five AA force fields (OPLS, L-OPLS, COMPASS, AIREBO-M, ReaxFF), three UA force fields (TraPPE, Potoff, TAMie), and one CG force field (MARTINI). The Potoff UA force field yields the best results for all three properties and is at the same time still computationally relatively cheap. The COMPASS and the ReaxFF AA force fields provide a good

accuracy predicting the density, the viscosity, and the self-diffusion coefficient. For all force fields (except AIREBO-M), the deviations from experimental data increase with increasing pressure. The reason that AIREBO-M AA force field performs relatively well at extreme pressure is probably due to the applied parametrization which included data at high pressure.[74] The CG force field MARTINI simplifies the molecular architecture most. It yields large deviations from experimental data. The unphysical prediction of a solid-like phase by the OPLS force field for long linear alkanes[72] was confirmed by our simulations. The optimized version for long linear alkanes of the OPLS force field, the L-OPLS force field,[72] shows significantly better results. If no experimental data are available, the predictions by the force fields can provide good estimates to fill this gap. The Potoff force field is recommended for this purpose. The accuracy of predictions of experimental data for the studied substances with this model was found to be about 0.5 % for the density, 10 % for the viscosity, and 18 % for the self-diffusion coefficient. As a convenient tool, also the empirical correlations developed in the present work based on the Potoff predictions can be used.

The results from this work can be taken as a benchmark for testing the performance of new force fields under extreme conditions.

Supporting Information Available

- Supplementary Material: Parameter studies (finite size, integrator, equilibration, cutoff criterion of the TDM method), additional evaluation of the simulations, and force field parameters.
- Simulation Data: Numeric simulation data.

Acknowledgement

The present research was conducted under the auspices of the Boltzmann-Zuse Society for

Computational Molecular Engineering (BZS). The simulations were carried out on the Elwe at Regional University Computing Center Kaiserslautern (RHRK) [grant TUK-MTD]. The project was funded by the Deutsche Forschungsgemeinschaft (DFG, German Research Foundation) – 252408385 - IRTG 2057 and by the Federal Ministry of Education and Research (BMBF, Germany) – 16ME0613 – WindHPC.

References

(1) Bair, S. A Traction (Friction) Curve Is Not a Flow Curve. *Lubricants* **2022**, *10*, 221.

(2) Stachowiak, G. W. How tribology has been helping us to advance and to survive. *Friction* **2017**, *5*, 233–247.

(3) Ahuja, A.; Lee, R.; Joshi, Y. M. Advances and challenges in the high-pressure rheology of complex fluids. *Advances in Colloid and Interface Science* **2021**, *294*, 102472.

(4) Ewen, J. P.; Spikes, H. A.; Dini, D. Contributions of Molecular Dynamics Simulations to Elastohydrodynamic Lubrication. *Tribology Letters* **2021**, *69*, 24.

(5) Jadhao, V.; Robbins, M. O. Probing large viscosities in glass-formers with nonequilibrium simulations. *Proceedings of the National Academy of Sciences* **2017**, *114*, 7952–7957.

(6) McCabe, C.; Cui, S.; Cummings, P. T. Characterizing the viscosity–temperature dependence of lubricants by molecular simulation. *Fluid Phase Equilibria* **2001**, *183-184*, 363–370.

(7) Liu, P.; Yu, H.; Ren, N.; Lockwood, F. E.; Wang, Q. J. Pressure–Viscosity Coefficient of Hydrocarbon Base Oil through Molecular Dynamics Simulations. *Tribology Letters* **2015**, *60*, 34.

(8) Kondratyuk, N. D.; Pisarev, V. V. Calculation of viscosities of branched alkanes from 0.1 to 1000 MPa by molecular dynamics methods using COMPASS force field. *Fluid Phase Equilibria* **2019**, *498*, 151–159.

(9) Mathas, D.; Holweger, W.; Wolf, M.; Bohnert, C.; Bakolas, V.; Procelewska, J.; Wang, L.; Bair, S.; Skylaris, C.-K. Evaluation of methods for viscosity simulations of lubricants at different temperatures and pressures: a case study on PAO-2. *Tribology Transactions* **2021**, *64*, 1138–1148.

(10) Kondratyuk, N. D.; Pisarev, V. V.; Ewen, J. P. Probing the high-pressure viscosity of hydrocarbon mixtures using molecular dynamics simulations. *The Journal of Chemical Physics* **2020**, *153*, 154502.

(11) Kondratyuk, N. D.; Pisarev, V. V. Predicting shear viscosity of 1,1-diphenylethane at high pressures by molecular dynamics methods. *Fluid Phase Equilibria* **2021**, *544-545*, 113100.

(12) Becker, S.; Urbassek, H. M.; Horsch, M.; Hasse, H. Contact Angle of Sessile Drops in Lennard-Jones Systems. *Langmuir* **2014**, *30*, 13606–13614.

(13) Heier, M.; Stephan, S.; Diewald, F.; Müller, R.; Langenbach, K.; Hasse, H. Molecular Dynamics Study of Wetting and Adsorption of Binary Mixtures of the Lennard-Jones Truncated and Shifted Fluid on a Planar Wall. *Langmuir* **2021**, *37*, 7405–7419.

(14) Vo, T. Q.; Park, B.; Park, C.; Kim, B. Nano-scale liquid film sheared between strong wetting surfaces: effects of interface region on the flow. *Journal of Mechanical Science and Technology* **2015**, *29*, 1681–1688.

(15) Schmitt, S.; Vo, T.; Lautenschlaeger, M. P.; Stephan, S.; Hasse, H. Molecular dynamics simulation study of heat transfer across solid–fluid interfaces in a simple model system. *Molecular Physics* **2022**, *120*, e2057364.

(16) Schmitt, S.; Stephan, S.; Kirsch, B.; Aurich, J. C.; Kerscher, E.; Urbassek, H. M.; Hasse, H. Molecular Simulation Study on the Influence of the Scratching Velocity on Nanoscopic Contact Processes. *2nd International Conference of the DFG International Research Training Group 2057 – Physical Modeling for Virtual Manufacturing (iPMVM 2020)* **2021**, *89*, 17:1–17:16.

(17) Stephan, S.; Dyga, M.; Urbassek, H. M.; Hasse, H. The Influence of Lubrication and the Solid–Fluid Interaction on Thermodynamic Properties in a Nanoscopic Scratching Process. *Langmuir* **2019**, *35*, 16948–16960.

(18) Stephan, S.; Lautenschlaeger, M. P.; Alhafez, I. A.; Horsch, M. T.; Urbassek, H. M.; Hasse, H. Molecular Dynamics Simulation Study of Mechanical Effects of Lubrication on a Nanoscale Contact Process. *Tribology Letters* **2018**, *66*, 126.

(19) Ta, T. D.; Tieu, A. K.; Zhu, H.; Kosasih, B.; Zhu, Q.; Phan, H. T. The structural, tribological, and rheological dependency of thin hexadecane film confined between iron and iron oxide surfaces under sliding conditions. *Tribology International* **2017**, *113*, 26–35.

(20) Gao, Y.; Brodyanski, A.; Kopnarski, M.; Urbassek, H. M. Nanoscratching of iron: A molecular dynamics study of the influence of surface orientation and scratching direction. *Computational Materials Science* **2015**, *103*, 77–89.

(21) Alhafez, I. A.; Ruestes, C. J.; Gao, Y.; Urbassek, H. M. Nanoindentation of hcp metals: a comparative simulation study of the evolution of dislocation networks. *Nanotechnology* **2016**, *27*, 045706.

(22) Washizu, H.; Ohmori, T.; Suzuki, A. Molecular origin of limiting shear stress of elastohydrodynamic lubrication oil film studied by molecular dynamics. *Chemical Physics Letters* **2017**, *678*, 1–4.

(23) Tromp, S.; Joly, L.; Cobian, M.; Fillot, N. Tribological Performance of the R1233zd Refrigerant in Extreme Confinement at the Nanoasperity Level: A Molecular Dynamics Study Using an ab Initio-Based Force Field. *Tribology Letters* **2019**, *67*, 67.

(24) Kioupis, L. I.; Maginn, E. J. Molecular Simulation of Poly-α-olefin Synthetic Lubricants: Impact of Molecular Architecture on Performance Properties. *The Journal of Physical Chemistry B* **1999**, *103*, 10781–10790.

(25) Kondratyuk, N.; Lenev, D.; Pisarev, V. Transport coefficients of model lubricants up to 400 MPa from molecular dynamics. *The Journal of Chemical Physics* **2020**, *152*, 191104.

(26) Ewen, J.; Gattinoni, C.; Thakkar, F.; Morgan, N.; Spikes, H.; Dini, D. A Comparison of Classical Force-Fields for Molecular Dynamics Simulations of Lubricants. *Materials* **2016**, *9*, 651.

(27) Fertig, D.; Hasse, H.; Stephan, S. Transport properties of binary Lennard-Jones mixtures: Insights from entropy scaling and conformal solution theory. *Journal of Molecular Liquids* **2022**, *367*, 120401.

(28) Fertig, D.; Stephan, S. Influence of dispersive long-range interactions on transport and excess properties of simple mixtures. *Molecular Physics* **2023**, *0*, e2162993.

(29) Liu, P.; Lu, J.; Yu, H.; Ren, N.; Lockwood, F. E.; Wang, Q. J. Lubricant shear thinning behavior correlated with variation of radius of gyration via molecular dynamics simulations. *The Journal of Chemical Physics* **2017**, *147*, 084904.

(30) Jadhao, V.; Robbins, M. O. Rheological Properties of Liquids Under Conditions of Elastohydrodynamic Lubrication. *Tribology Letters* **2019**, *67*, 66.

(31) Pisarev, V.; Kondratyuk, N. Prediction of viscosity-density dependence of liquid methane+n-butane+n-pentane mixtures using the molecular dynamics method and empirical correlations. *Fluid Phase Equilibria* **2019**, *501*, 112273.

(32) Galvani Cunha, M. A.; Robbins, M. O. Determination of pressure-viscosity relation of 2,2,4-trimethylhexane by all-atom molecular dynamics simulations. *Fluid Phase Equilibria* **2019**, *495*, 28–32.

(33) Zhang, Y.; Otani, A.; Maginn, E. J. Reliable Viscosity Calculation from Equilibrium Molecular Dynamics Simulations: A Time Decomposition Method. *Journal of Chemical Theory and Computation* **2015**, *11*, 3537–3546.

(34) Ewen, J. P.; Heyes, D. M.; Dini, D. Advances in nonequilibrium molecular dynamics simulations of lubricants and additives. *Friction* **2018**, *6*, 349–386.

(35) Bair, S. The high pressure rheology of some simple model hydrocarbons. *Proceedings of the Institution of Mechanical Engineers, Part J: Journal of Engineering Tribology* **2002**, *216*, 139–149.

(36) Harrison, J. A.; Schall, J. D.; Maskey, S.; Mikulski, P. T.; Knippenberg, M. T.; Morrow, B. H. Review of force fields and intermolecular potentials used in atomistic computational materials research. *Applied Physics Reviews* **2018**, *5*, 031104.

(37) Morrow, B. H.; Harrison, J. A. Evaluating the Ability of Selected Force Fields to Simulate Hydrocarbons as a Function of Temperature and Pressure Using Molecular Dynamics. *Energy & Fuels* **2021**, *35*, 3742 – 3752.

(38) Stephan, S.; Horsch, M. T.; Vrabec, J.; Hasse, H. MolMod – an open access database of force fields for molecular simulations of fluids. *Molecular Simulation* **2019**, *45*, 806–814.

(39) Benda, R.; Bullen, J.; Plomer, A. Synthetics basics: Polyalphaolefins — base fluids for high-performance lubricants. *Journal of Synthetic Lubrication* **1996**, *13*, 41–57.

(40) Bürk, V.; Pollak, S.; Quiñones-Cisneros, S. E.; Schmidt, K. A. G. Complementary Experimental Data and Extended Density and Viscosity Reference Models for Squalane. *Journal of Chemical & Engineering Data* **2021**, *66*, 1992 – 2005.

(41) Ciriminna, R.; Pandarus, V.; Béland, F.; Pagliaro, M. Catalytic Hydrogenation of Squalene to Squalane. *Organic Process Research & Development* **2014**, *18*, 1110–1115.

(42) Verma, A.; Cracknell, R.; Doyle, D.; Rudra, I. Determination of Diesel Physical Properties at Injection Pressures and Temperatures via All-Atom Molecular Simulations. *SAE International Journal of Fuels and Lubricants* **2016**, *9*, 567–574.

(43) Burrows, S. A.; Korotkin, I.; Smoukov, S. K.; Boek, E.; Karabasov, S. Benchmarking of

Molecular Dynamics Force Fields for Solid–Liquid and Solid–Solid Phase Transitions in Alkanes. *The Journal of Physical Chemistry B* **2021**, *125*, 5145 – 5159.

(44) Oliveira, M. P.; Gonçalves, Y. M. H.; Ol Gheta, S. K.; Rieder, S. R.; Horta, B. A. C.; Hünenberger, P. H. Comparison of the United- and All-Atom Representations of (Halo)alkanes Based on Two Condensed-Phase Force Fields Optimized against the Same Experimental Data Set. *Journal of Chemical Theory and Computation* **2022**, *18*, 6757–6778.

(45) Hamani, A. W. S.; Bazile, J.-P.; Hoang, H.; Luc, H. T.; Daridon, J.-L.; Galliero, G. Thermophysical properties of simple molecular liquid mixtures: On the limitations of some force fields. *Journal of Molecular Liquids* **2020**, *303*, 112663.

(46) da Silva, G. C. Q.; Silva, G. M.; Tavares, F. W.; Fleming, F. P.; Horta, B. A. C. Are all-atom any better than united-atom force fields for the description of liquid properties of alkanes? *Journal of Molecular Modeling* **2020**, *26*, 296.

(47) Papavasileiou, K. D.; Peristeras, L. D.; Bick, A.; Economou, I. G. Molecular Dynamics Simulation of Pure *n*-Alkanes and Their Mixtures at Elevated Temperatures Using Atomistic and Coarse-Grained Force Fields. *The Journal of Physical Chemistry B* **2019**, *123*, 6229–6243.

(48) Lin, L.; Kedzierski, M. A. Density and viscosity of a polyol ester lubricant: Measurement and molecular dynamics simulation. *International Journal of Refrigeration* **2020**, *118*, 188–201.

(49) Messerly, R. A.; Anderson, M. C.; Razavi, S. M.; Elliott, J. R. Improvements and limitations of Mie λ-6 potential for prediction of saturated and compressed liquid viscosity. *Fluid Phase Equilibria* **2019**, *483*, 101–115.

(50) Saager, B.; Fischer, J. Predictive power of effective intermolecular pair potentials:

MD simulation results for methane up to 1000 MPa. *Fluid Phase Equilibria* **1990**, *57*, 35–46.

(51) Welling, U.; Germano, G. Efficiency of linked cell algorithms. *Computer Physics Communications* **2011**, *182*, 611–615.

(52) Plimpton, S. J.; Thompson, A. P. Computational aspects of many-body potentials. *MRS Bulletin* **2012**, *37*, 513–521.

(53) Toukmaji, A. Y.; Board, J. A. Ewald summation techniques in perspective: a survey. *Computer Physics Communications* **1996**, *95*, 73–92.

(54) Tuckerman, M.; Berne, B. J.; Martyna, G. J. Reversible multiple time scale molecular dynamics. *The Journal of Chemical Physics* **1992**, *97*, 1990–2001.

(55) Allen, M. P.; Tildesley, D. J. *Computer Simulation of Liquids*, 2nd ed.; Oxford University Press: Oxford, United Kingdom, 2017.

(56) Ryckaert, J.-P.; Ciccotti, G.; Berendsen, H. J. Numerical integration of the cartesian equations of motion of a system with constraints: molecular dynamics of n-alkanes. *Journal of Computational Physics* **1977**, *23*, 327–341.

(57) Pollock, E.; Glosli, J. Comments on P3M, FMM, and the Ewald method for large periodic Coulombic systems. *Computer Physics Communications* **1996**, *95*, 93–110.

(58) Thompson, A. P.; Aktulga, H. M.; Berger, R.; Bolintineanu, D. S.; Brown, W. M.; Crozier, P. S.; in 't Veld, P. J.; Kohlmeyer, A.; Moore, S. G.; Nguyen, T. D. et al. LAMMPS - a flexible simulation tool for particle-based materials modeling at the atomic, meso, and continuum scales. *Computer Physics Communications* **2022**, *271*, 108171.

(59) Nosé, S. A molecular dynamics method for simulations in the canonical ensemble. *Molecular Physics* **1984**, *52*, 255–268.

(60) Hoover, W. G. Canonical dynamics: Equilibrium phase-space distributions. *Physical Review A* **1985**, *31*, 1695–1697.

(61) Shinoda, W.; Shiga, M.; Mikami, M. Rapid estimation of elastic constants by molecular dynamics simulation under constant stress. *Physical Review B* **2004**, *69*, 134103.

(62) Green, M. S. Markoff Random Processes and the Statistical Mechanics of Time-Dependent Phenomena. II. Irreversible Processes in Fluids. *The Journal of Chemical Physics* **1954**, *22*, 398–413.

(63) Kubo, R. Statistical-Mechanical Theory of Irreversible Processes. I. General Theory and Simple Applications to Magnetic and Conduction Problems. *Journal of the Physical Society of Japan* **1957**, *12*, 570–586.

(64) Calandrini, V.; Pellegrini, E.; Calligari, P.; Hinsen, K.; Kneller, G. R. nMoldyn - Interfacing spectroscopic experiments, molecular dynamics simulations and models for time correlation functions. *École thématique de la Société Française de la Neutronique* **2011**, *12*, 201–232.

(65) Liu, H.; Maginn, E.; Visser, A. E.; Bridges, N. J.; Fox, E. B. Thermal and Transport Properties of Six Ionic Liquids: An Experimental and Molecular Dynamics Study. *Industrial & Engineering Chemistry Research* **2012**, *51*, 7242–7254.

(66) Hess, B. Determining the shear viscosity of model liquids from molecular dynamics simulations. *The Journal of Chemical Physics* **2002**, *116*, 209.

(67) Mondello, M.; Grest, G. S. Viscosity calculations of n-alkanes by equilibrium molecular dynamics. *The Journal of Chemical Physics* **1997**, *106*, 9327–9336.

(68) Moultos, O. A.; Zhang, Y.; Tsimpanogiannis, I. N.; Economou, I. G.; Maginn, E. J. System-size corrections for self-diffusion coefficients calculated from molecular dynam-

ics simulations: The case of CO_2, n-alkanes, and poly(ethylene glycol) dimethyl ethers. *The Journal of Chemical Physics* **2016**, *145*, 074109.

(69) Yeh, I.-C.; Hummer, G. System-Size Dependence of Diffusion Coefficients and Viscosities from Molecular Dynamics Simulations with Periodic Boundary Conditions. *The Journal of Physical Chemistry B* **2004**, *108*, 15873–15879.

(70) Jorgensen, W. L.; Maxwell, D. S.; Tirado-Rives, J. Development and Testing of the OPLS All-Atom Force Field on Conformational Energetics and Properties of Organic Liquids. *Journal of the American Chemical Society* **1996**, *118*, 11225–11236.

(71) Sun, H. COMPASS: An ab Initio Force-Field Optimized for Condensed-Phase ApplicationssOverview with Details on Alkane and Benzene Compounds. *The Journal of Physical Chemistry B* **1998**, *102*, 7338–7364.

(72) Siu, S. W. I.; Pluhackova, K.; Böckmann, R. A. Optimization of the OPLS-AA Force Field for Long Hydrocarbons. *Journal of Chemical Theory and Computation* **2012**, *8*, 1459–1470.

(73) Zhang, W.; van Duin, A. C. T. Improvement of the ReaxFF Description for Functionalized Hydrocarbon/Water Weak Interactions in the Condensed Phase. *The Journal of Physical Chemistry B* **2018**, *122*, 4083–4092.

(74) O'Connor, T. C.; Andzelm, J.; Robbins, M. O. AIREBO-M: A reactive model for hydrocarbons at extreme pressures. *The Journal of Chemical Physics* **2015**, *142*, 024903.

(75) Martin, M. G.; Siepmann, J. I. Transferable Potentials for Phase Equilibria. 1. United-Atom Description of n-Alkanes. *The Journal of Physical Chemistry B* **1998**, *102*, 2569–2577.

(76) Martin, M. G.; Siepmann, J. I. Novel Configurational-Bias Monte Carlo Method for Branched Molecules. Transferable Potentials for Phase Equilibria. 2. United-Atom

Description of Branched Alkanes. *The Journal of Physical Chemistry B* **1999**, *103*, 4508–4517.

(77) Potoff, J. J.; Bernard-Brunel, D. A. Mie Potentials for Phase Equilibria Calculations: Application to Alkanes and Perfluoroalkanes. *The Journal of Physical Chemistry B* **2009**, *113*, 14725–14731.

(78) Mick, J. R.; Soroush Barhaghi, M.; Jackman, B.; Schwiebert, L.; Potoff, J. J. Optimized Mie Potentials for Phase Equilibria: Application to Branched Alkanes. *Journal of Chemical & Engineering Data* **2017**, *62*, 1806–1818.

(79) Hemmen, A.; Gross, J. Transferable Anisotropic United-Atom Force Field Based on the Mie Potential for Phase Equilibrium Calculations: n-Alkanes and n-Olefins. *The Journal of Physical Chemistry B* **2015**, *119*, 11695–11707.

(80) Weidler, D.; Gross, J. Individualized force fields for alkanes, olefins, ethers and ketones based on the transferable anisotropic Mie potential. *Fluid Phase Equilibria* **2018**, *470*, 101–108.

(81) Marrink, S. J.; Risselada, H. J.; Yefimov, S.; Tieleman, D. P.; de Vries, A. H. The MARTINI Force Field: Coarse Grained Model for Biomolecular Simulations. *The Journal of Physical Chemistry B* **2007**, *111*, 7812–7824.

(82) van Duin, A. C. T.; Dasgupta, S.; Lorant, F.; Goddard, W. A. ReaxFF: A Reactive Force Field for Hydrocarbons. *The Journal of Physical Chemistry A* **2001**, *105*, 9396–9409.

(83) Stuart, S. J.; Tutein, A. B.; Harrison, J. A. A reactive potential for hydrocarbons with intermolecular interactions. *The Journal of Chemical Physics* **2000**, *112*, 6472–6486.

(84) MacKerell, A. D.; Bashford, D.; Bellott, M.; Dunbrack, R. L.; Evanseck, J. D.; Field, M. J.; Fischer, S.; Gao, J.; Guo, H.; Ha, S. et al. All-Atom Empirical Potential

for Molecular Modeling and Dynamics Studies of Proteins. *The Journal of Physical Chemistry B* **1998**, *102*, 3586–3616.

(85) Rane, K. S.; Murali, S.; Errington, J. R. Monte Carlo Simulation Methods for Computing Liquid–Vapor Saturation Properties of Model Systems. *Journal of Chemical Theory and Computation* **2013**, *9*, 2552–2566.

(86) Patel, S.; Wilding, W. V.; Rowley, R. L. The use of two-phase molecular dynamics simulations to determine the phase behavior and critical point of propane molecular models. *The Journal of Chemical Physics* **2011**, *134*, 024101.

(87) Gordon, P. A. Development of intermolecular potentials for predicting transport properties of hydrocarbons. *The Journal of Chemical Physics* **2006**, *125*, 014504.

(88) Fischer, M.; Bauer, G.; Gross, J. Force Fields with Fixed Bond Lengths and with Flexible Bond Lengths: Comparing Static and Dynamic Fluid Properties. *Journal of Chemical & Engineering Data* **2020**, *65*, 1583 – 1593.

(89) Jorgensen, W. L.; Madura, J. D.; Swenson, C. J. Optimized intermolecular potential functions for liquid hydrocarbons. *Journal of the American Chemical Society* **1984**, *106*, 6638–6646.

(90) Jarin, Z.; Newhouse, J.; Voth, G. A. Coarse-Grained Force Fields from the Perspective of Statistical Mechanics: Better Understanding of the Origins of a MARTINI Hangover. *Journal of Chemical Theory and Computation* **2021**, *17*, 1170–1180.

(91) Bereau, T.; Kremer, K. Automated Parametrization of the Coarse-Grained Martini Force Field for Small Organic Molecules. *Journal of Chemical Theory and Computation* **2015**, *11*, 2783–2791.

(92) Graham, J. A.; Essex, J. W.; Khalid, S. PyCGTOOL: Automated Generation of

Coarse-Grained Molecular Dynamics Models from Atomistic Trajectories. *Journal of Chemical Information and Modeling* **2017**, *57*, 650–656.

(93) Potter, T. D.; Barrett, E. L.; Miller, M. A. Automated Coarse-Grained Mapping Algorithm for the Martini Force Field and Benchmarks for Membrane–Water Partitioning. *Journal of Chemical Theory and Computation* **2021**, *17*, 5777–5791.

(94) Souza, P. C. T.; Alessandri, R.; Barnoud, J.; Thallmair, S.; Faustino, I.; Grünewald, F.; Patmanidis, I.; Abdizadeh, H.; Bruininks, B. M. H.; Wassenaar, T. A. et al. Martini 3: a general purpose force field for coarse-grained molecular dynamics. *Nature Methods* **2021**, *18*, 382–388.

(95) Liu, K.; Wu, Y.; McHugh, M. A.; Baled, H.; Enick, R. M.; Morreale, B. D. Equation of state modeling of high-pressure, high-temperature hydrocarbon density data. *The Journal of Supercritical Fluids* **2010**, *55*, 701–711.

(96) Caudwell, D. R.; Trusler, J. P. M.; Vesovic, V.; Wakeham, W. A. Viscosity and Density of Five Hydrocarbon Liquids at Pressures up to 200 MPa and Temperatures up to 473 K. *Journal of Chemical & Engineering Data* **2009**, *54*, 359–366.

(97) Audonnet, F.; Pádua, A. A. H. Viscosity and density of mixtures of methane and n-decane from 298 to 393 K and up to 75 MPa. *Fluid Phase Equilibria* **2004**, *216*, 235–244.

(98) Oliveira, C. M. B. P.; Wakeham, W. A. The viscosity of five liquid hydrocarbons at pressures up to 250 MPa. *International Journal of Thermophysics* **1992**, *13*, 773–790.

(99) Doolittle, A. K. Specific Volumes of n -Alkanes. *Journal of Chemical & Engineering Data* **1964**, *9*, 275–279.

(100) Wu, Y.; Bamgbade, B.; Liu, K.; McHugh, M. A.; Baled, H.; Enick, R. M.; Burgess, W. A.; Tapriyal, D.; Morreale, B. D. Experimental measurements and equa-

tion of state modeling of liquid densities for long-chain n-alkanes at pressures to 265MPa and temperatures to 523K. *Fluid Phase Equilibria* **2011**, *311*, 17–24.

(101) Ciotta, F.; Maitland, G.; Smietana, M.; Trusler, J. P. M.; Vesovic, V. Viscosity and Density of Carbon Dioxide + 2,6,10,15,19,23-Hexamethyltetracosane (Squalane). *Journal of Chemical & Engineering Data* **2010**, *55*, 4126–4126.

(102) Rowane, A. J.; Mallepally, R. R.; Gupta, A.; Gavaises, M.; McHugh, M. A. High-Temperature, High-Pressure Viscosities and Densities of *n* -Hexadecane, 2,2,4,4,6,8,8-Heptamethylnonane, and Squalane Measured Using a Universal Calibration for a Rolling-Ball Viscometer/Densimeter. *Industrial & Engineering Chemistry Research* **2019**, *58*, 4303–4316.

(103) Bamgbade, B. A.; Wu, Y.; Burgess, W. A.; Tapriyal, D.; Gamwo, I. K.; Baled, H. O.; Enick, R. M.; McHugh, M. A. High-Temperature, High-Pressure Volumetric Properties of Propane, Squalane, and Their Mixtures: Measurement and PC-SAFT Modeling. *Industrial & Engineering Chemistry Research* **2015**, *54*, 6804–6811.

(104) Schmidt, K. A. G.; Pagnutti, D.; Curran, M. D.; Singh, A.; Trusler, J. P. M.; Maitland, G. C.; McBride-Wright, M. New Experimental Data and Reference Models for the Viscosity and Density of Squalane. *Journal of Chemical & Engineering Data* **2015**, *60*, 137–150.

(105) Naake, L.-D.; Wiegand, G.; Franck, E. U. The Viscosity of n-Decane to High Temperatures of 573 K and High Pressures of 300 MPa. *Zeitschrift für Physikalische Chemie* **2002**, *216*, 1295 – 1310.

(106) Baled, H. O.; Xing, D.; Katz, H.; Tapriyal, D.; Gamwo, I. K.; Soong, Y.; Bamgbade, B. A.; Wu, Y.; Liu, K.; McHugh, M. A. et al. Viscosity of n-hexadecane, n-octadecane and n-eicosane at pressures up to 243MPa and temperatures up to 534K. *The Journal of Chemical Thermodynamics* **2014**, *72*, 108–116.

(107) Bair, S. Reference liquids for quantitative elastohydrodynamics: selection and rheological characterization. *Tribology Letters* **2006**, *22*, 197–206.

(108) Suárez-Iglesias, O.; Medina, I.; Sanz, M.; Pizarro, C.; Bueno, J. L. Self-Diffusion in Molecular Fluids and Noble Gases: Available Data. *Journal of Chemical & Engineering Data* **2015**, *60*, 2757–2817.

(109) Vardag, T.; Karger, N.; Lüdemann, H.-D. Temperature and Pressure Dependence of Self Diffusion in Long Liquid n-Alkanes. *Berichte der Bunsengesellschaft für physikalische Chemie* **1991**, *95*, 859–865.

(110) Thomas, L. L.; Christakis, T. J.; Jorgensen, W. L. Conformation of Alkanes in the Gas Phase and Pure Liquids. *The Journal of Physical Chemistry B* **2006**, *110*, 21198–21204.

(111) Moultos, O. A.; Tsimpanogiannis, I. N.; Panagiotopoulos, A. Z.; Trusler, J. P. M.; Economou, I. G. Atomistic Molecular Dynamics Simulations of Carbon Dioxide Diffusivity in n-Hexane, n-Decane, n-Hexadecane, Cyclohexane, and Squalane. *The Journal of Physical Chemistry B* **2016**, *120*, 12890–12900.

(112) Kondratyuk, N. D. Comparing different force fields by viscosity prediction for branched alkane at 0.1 and 400 MPa. *Journal of Physics: Conference Series* **2019**, *1385*, 012048.

(113) Einstein, A. Über die von der molekularkinetischen Theorie der Wärme geforderte Bewegung von in ruhenden Flüssigkeiten suspendierten Teilchen. *Annalen der Physik* **1905**, *322*, 549–560.

(114) dos Santos, T. J.; Abreu, C. R.; Horta, B. A.; Tavares, F. W. Self-diffusion coefficients of methane/n-hexane mixtures at high pressures: An evaluation of the finite-size effect and a comparison of force fields. *The Journal of Supercritical Fluids* **2020**, *155*, 104639.

Graphical TOC Entry